Letter

The effect of external electric field on the performance of perovskite solar cells

Xiaodong Li [a,c], Xueyan Wang [a,c], Wenjun Zhang [a], Yulei Wu [a], Feng Gao [b,*], Junfeng Fang [a,*]

[a] Ningbo Institute of Materials Technology and Engineering, Chinese Academy of Sciences, Ningbo 315201, China
[b] Department of Physics, Biology and Chemistry (IFM), Linköping University, Linköping SE-581 83, Sweden
[c] University of Chinese Academy of Sciences, Beijing 100049, China

ARTICLE INFO

Keywords:
Perovskite solar cells
External bias
Ion motion
Electric double layers

ABSTRACT

Planar heterojunction perovskite solar cells were fabricated through a low temperature approach. We find that the device performance significantly depends on the external bias before and during measurements. By appropriate optimization of the bias conditions, we could achieve an 8-fold increase in the power conversion efficiency. The significant improvement in device performance might be caused by the ion motion in the perovskite under the external electric field.

1. Introduction

The perovskite based materials ($CH_3NH_3PbX_3$, X = halogen) have attracted much interest for their promising application in solar cells as the light-absorbing component [1–3]. Initially, the perovskite solar cells employed an architecture similar to dye-sensitized solar cells (DSSCs) and a power conversion efficiency (PCE) of 3–4% was obtained [4]. Recently, with the optimization of device structure and materials design, substantial progress has been made [5–8], leading to the PCE exceeding 15% [7]. For this type of solar cells, the mesoporous metal oxides provide a scaffold on which the perovskite materials are grown. In addition, the scaffold also facilitates the electron transport from perovskite light-absorber to the electrodes [6,7]. Despite the high PCE, the mesoporous metal oxides usually require high temperature (~500 °C) to sinter, which is not compatible with flexible substrates.

Recently, Snaith and co-workers demonstrated that the planar heterojunction perovskite solar cells without mesoporous scaffold could also show a high PCE of 15.4% by a vapour deposition approach [9]. And the PCE up to 11.4% was also obtained through solution fabrication [10]. Compared with the previous DSSC structure with mesoporous scaffold, the planar heterojunction perovskite solar cells could be fabricated with much simpler process. However, for most state-of-the-art planar heterojunction perovskite solar cells, the perovskite light-absorber was deposited on a compact TiO_2 layer, which also required high temperature to sinter or crystallize [9–12]. Essentially, these planar heterojunction perovskite solar cells did not completely avoid the problems of high temperature mentioned above.

Soon afterwards, Jeng et al. demonstrated another type of planar heterojunction perovskite solar cells [13]. The perovskite materials were deposited on the ITO/PEDOT:PSS substrate, which made the structure similar to organic solar cells. Despite the relative moderate PCE of 3.9%, the easy fabrication and no need of high temperature treatment are attractive for decreasing the fabrication cost.

* Corresponding authors.
E-mail addresses: fenga@ifm.liu.se (F. Gao), fangjf@nimte.ac.cn (J. Fang).

Afterwards, Sun et al. increased the PCE to 7.4% through two-step deposition of perovskite materials [14]. In addition, the groups of Snaith, Yang and Bolink also reported low temperature fabricated planar perovskite solar cells and PCEs approaching or over 10% were obtained [15–18]. In such a short time (less than 1 year), the PCE of planar heterojunction perovskite solar cells significantly increased from ~4% to over 10%, indicating promising future for planar perovskite solar cells.

In spite of significant improvement in device performance of perovskite solar cells, understanding of the operation mechanisms is still in progress [19–21]. For example, the mechanisms behind efficient charge generation, high open-circuit voltage, and anomalous hysteresis in the *J–V* curves are not clear yet. Here, we fabricated planar perovskite solar cells on the ITO/PEDOT:PSS substrates (Fig. 1). We found that the external bias plays a critical role on the device performance. By applying an external bias prior to the device measurement, the PCE could be significantly increased from ~1% to over 8%. In addition, the test conditions, e.g. the scan bias range, could also effectively affect device performance. We propose that that the ion motion in the perovskite might be responsible for the behavior observed.

2. Material and methods

2.1. Synthesis of CH_3NH_3I

CH_3NH_3I was synthesized through the reaction of 24 mL methylamine (33 wt.% in ethanol, Aldrich) and 10 mL hydroiodic acid (57 wt.% in water, Aladdin, China) in 100 mL ethanol at ice bath for 2 h with stirring. The precipitate was collected with a rotary evaporator at 50 °C to exclude the solvent. Then the produce was recrystallized in ethanol. The crystals were filtered and washed with diethyl ether three times. At last, the solid was dried at 60 °C in vacuum oven overnight.

2.2. Fabrication of perovskite solar cells

ITO glass was cleaned with ultrasonic treatment in deionized water, acetone and isopropanol for 15 min, respectively. Then the substrates were dried with N_2 flow and further cleaned with UV–ozone for 20 min. Next, PEDOT:PSS (Clevios 4083) was spin-coated on ITO substrates at 4000 rpm 60 s and heated at 140 °C 15 min in air. After that, the substrates were transferred to glovebox (filled with N_2). Perovskite precursor solution was prepared by dissolved CH_3NH_3I and $PbCl_2$ with molar ratio of 3:1 in DMF (40 wt.%) at 60 °C. Then the solution was deposited on ITO by spin-coating at 2000 rpm for 45 s. After spin-coating, the substrates were left in glovebox for 1 h, and then annealed at 100 °C for 1 h. At last, the substrates were transferred to vacuum chamber (10^{-6} mbar) and 20 nm fullerene (C60, Aldrich) and 100 nm Al was deposited as cathode. The device area was 4 mm^2.

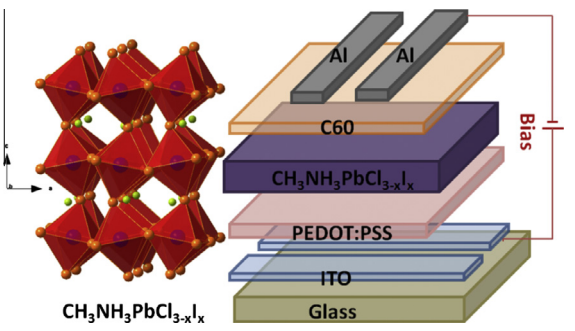

Fig. 1. The structure of the perovskite ($CH_3NH_3PbCl_{3-x}I_x$) and the device configuration used in our work.

2.3. Device characterization

The *J–V* measurements were carried out using Keithley 2440 sourcemeter controlled by a computer. All the solar cells were measured under simulated AM 1.5G spectrum (100 mW/cm^2) with an Oriel So13A solar simulator. Note that all the devices were measured from positive bias to negative bias.

3. Results and discussion

Fig. 2 shows the *J–V* curves with different scan bias range (the scans are from the positive bias to negative bias) for the same device. The fresh device shows poor performance (PCE of 0.13%) under −1 to 1 V scan range, mainly due to the inferior V_{oc} of 0.183 V, J_{sc} of 2.59 mA/cm^2, FF of 27.0%. When we measure the device with scan range of −1 to 2 V, the V_{oc} (0.445 V), J_{sc} (9.04 mA/cm^2), and FF (32.9%) all increase, leading to a moderate PCE of 1.32%. And when the scan range of −1 to 6 V is applied, a PCE of 4.29% is obtained with a V_{oc} of 0.708 V, J_{sc} of 15.34 mA/cm^2, and FF of 39.5%. However, when larger scan range of −1 to 8 V is applied, both the V_{oc} (0.695 V) and FF (37.0%) decrease, resulting in a decreased PCE of 4.04% despite slightly increased J_{sc} of 15.71 mA/cm^2. All the results above clearly indicate that the scan bias range plays a critical role on the device performance. The larger scan bias range leads to better performance (from 0.13% at −1 to 1 V to 4.29% at −1 to 6 V). But if the scan bias range is too large (e.g. −1 to 8 V), the large injection current density may destroy the device, thus resulting in decreased performance.

To further understand the effect of external bias on device performance, we directly apply a bias on the device before the measurement (the direction of bias is shown in Fig. 1). The external bias is applied on the devices under dark conditions. We first investigate the effect of the bias direction on device performance (Fig. S1) and find that positive bias could significantly improve device performance, while negative bias decreases the performance, which agrees with the enhanced performance under large positive scan bias range mentioned in Fig. 2. We then turn to the relation between the bias value and device performance, and the results are shown in Fig. 3. The fresh device under the scan bias range of −0.5 V to 1.5 V shows poor performance with PCE of 0.79%. When a constant positive bias of 1 V is applied on the same device for 30 s, the performance could be slightly increased and a PCE of 1.10% is

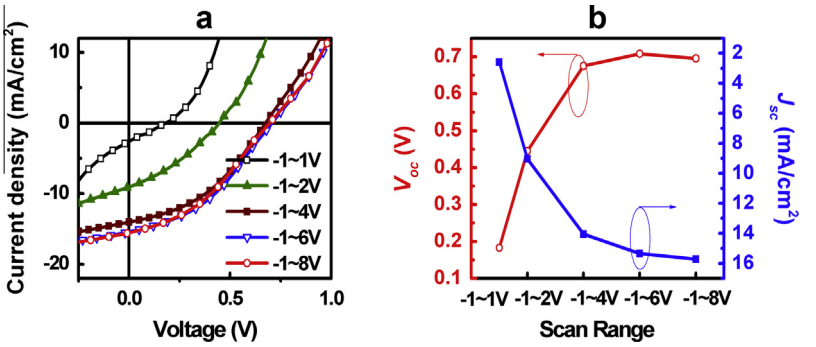

Fig. 2. (a) *J–V* curves, and (b) V_{oc} and J_{sc} values under different scan bias range. The scans are from the positive bias to negative bias.

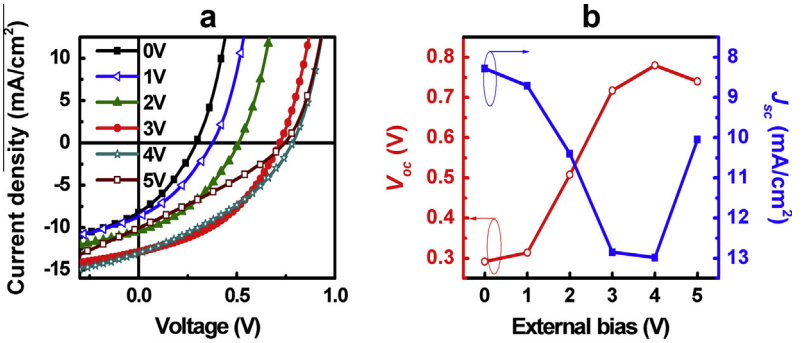

Fig. 3. (a) *J–V* curves, and (b) V_{oc} and J_{sc} values under different external bias for 30 s using the same scan range (−0.5 to 1.5 V).

obtained. And when a 3 V bias is applied for 30 s, the PCE could greatly increase to 3.89%, due to the much enhanced V_{oc} (0.717 V), J_{sc} (12.85 mA/cm^2) and FF (42.2%). When a larger bias of 5 V is applied for 30 s, the J_{sc} (10.05 mA/cm^2) and FF (29.7%) decrease, indicating that the device has already been destroyed. This phenomenon is consistent with the situation in scan range measurements, where larger scan range also destroys the device. From the above results, we can conclude that 3 V is the optimized bias for enhanced performance.

In addition, we also study the relation between the bias time (biased at 3 V) and device performance (Fig. S2). The fresh device shows PCE of 0.59% under −0.5 to 1.5 V. When the 3 V bias is applied for 5 s, the PCE slightly increased to 0.86%. If the bias time is increased to 10 s, the PCE could reach 1.5% with improved V_{oc} and J_{sc}. With further increasing bias time (20 s), the V_{oc} and J_{sc} continue increasing and a PCE of 2.71% is obtained. When the bias time is 40 s, the PCE is improved to 4.94%, due to the much improved V_{oc} (0.775 V), J_{sc} (14.70 mA/cm^2) and FF (43.4%). If longer time such as 80 s or 100 s is applied, the PCE decreases due to the significant decrease of FF, despite the slightly increased V_{oc}. As shown in Fig. S2 a bias of 3 V for 40 s is an optimized condition for good performance. One may argue that the performance enhancement is due to light soaking [22,23]. In order distinguish whether the enhancement is from light soaking effect or from the bias, we compare the performance of two fresh devices under the same scan bias range of −0.5 V to 1.5 V (Fig. S3). One device is measured after 3 V bias in the dark, while the other is measured after both 3 V bias and illumination under AM 1.5G spectrum. The two devices show almost the same performance, indicating that the external bias plays a major role in performance improvement and the light soaking effect is negligible.

Considering that both scan bias range and constant external bias could significantly improve device performance, we further proceed to investigate how these two factors combined would affect the device efficiency. As shown in Fig. 4, a typical fresh device shows inferior performance under −0.5 to 1.5 V. When we extend the scan range to −0.5 to 6 V, the device demonstrates significantly

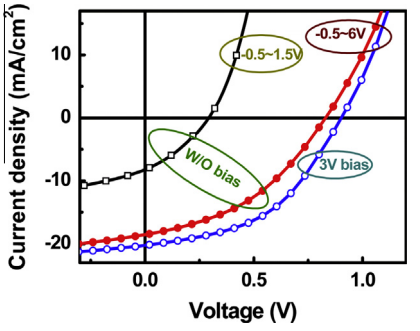

Fig. 4. The device response under different test conditions: applying an external bias or using different scan bias range.

improved performance (V_{oc} = 0.830 V, J_{sc} = 18.52 mA/cm^2, FF = 41.0% and PCE = 6.30%). When a 3 V bias is applied for 40 s prior to the measurement, a further improved performance (PCE = 8.55%) is obtained under the scan range of −0.5 to 6 V, with a high V_{oc} of 0.902 V, J_{sc} of 20.19 mA/cm^2, FF of 46.9% (the statistical analysis of device performance is shown in Fig. S4).

The *J*–*V* characteristics of devices under the dark conditions (Fig. S5) are also studied. For the fresh devices without pre-bias treatment, the obtained *J*–*V* curve shows poor diode characteristics, in agreement with the inferior device performance. After 3 V bias treatment, the device shows efficiently suppressed leakage current and much larger injection current, thus leading to obvious increase of the device rectification.

All the results above indicate that the external bias plays a critical role on the performance of perovskite solar cells. As a starting point, we examine whether impurities or poor morphology contributes to the bias-dependent behavior. We compare the X-ray diffraction (XRD) spectrum of the final product (the perovskite) and those of the starting materials ($PbCl_2$, PbI_2, and CH_3NH_3I). As shown in Fig. 5a, the XRD spectrum of the perovskite shows sharp (1 1 0) (2 2 0) peaks, consistent with previous reports [5,24]. No peaks from the starting materials could be detected in the final product, demonstrating that the perovskite contains negligible impurities. We also measured the surface and cross-section SEM images of the device (Fig. 5b and c). The perovskite layer is uniform, without any obvious pinholes, indicating high quality films in terms of morphology. XRD and SEM measurements exclude the possibilities that impurities or poor morphology affects the device performance.

Actually, our finding is similar to the hysteresis in *J*–*V* curves reported very recently by Snaith et al. [25], who proposed three possible mechanisms to explain the bias-dependent behavior: 1, ionic transport in perovskites; 2, trap states in perovskites; or 3, ferroelectric nature of perovskites. In order to further investigate the possible effects causing the phenomenon mentioned above, we proceeded to investigate the dark current transients (Fig. 6(a–c)). Dark current transients have been demonstrated to be useful to understand the effects of ions and traps in solar cells [26] as well as light-emitting electrochemical cells (LECs) [27–29]. When 1 V or 3 V bias is applied on the device, the current keeps decreasing with applying time of external bias. This could be due to trapping effects, with traps decreasing the current [26]. It could also be due to the reorientation or migration of ions [27–29]. Under the external bias, the ion reorientation or migration could form a reverse electric field, leading to the reduced current. When the bias is increased to 5 V, the situation becomes different. After a quick decrease, a rapid increase of the current appears. This observation is less likely to be caused by traps or ions reorientation. Instead, it could be well understood by considering ions migration in perovskite. Actually, this observation is quite similar to that in LECs [28], where the increase of the current is ascribed to doping of the polymer following the formation of electric double layers [27,29,30]. We propose that similar mechanisms might be involved in our perovskite solar cells. After the electrical double layer formation, halide ions might help the doping of perovskites or even improve the interface properties and hence increase the current. In addition, the rather large injection current under 5 V may destroy the device, which agrees with the results in Fig. 3. Since the ion migration beyond the electric double layer formation is detrimental to the device performance, the positive effect of the external bias on the device performance is only obtained during the electric double layer formation process, and hence might be short-lived.

In order to further understand the effect of ions, we measured impedance spectroscopy of our perovskite cells (the Nyquist plot shown in Fig. 6d). Linear increase in the low-frequency region demonstrates Warburg impedance, which indicates the existence of diffusion process (probably ions) in the cells [31,32]. This result is consistent with recent studies on the impedance spectroscopic analysis of $CH_3NH_3PbX_3$ sensitized solid-state solar cells, which also indicated the possibility of ionic transport in organometal trihalide perovskites [20,32]. Actually, the ionic motion in halide perovskites is nothing new. More than three decades ago, it has been demonstrated that $CsPbI_3$ is an ionic conductor, and that the ionic conduction is from the halide

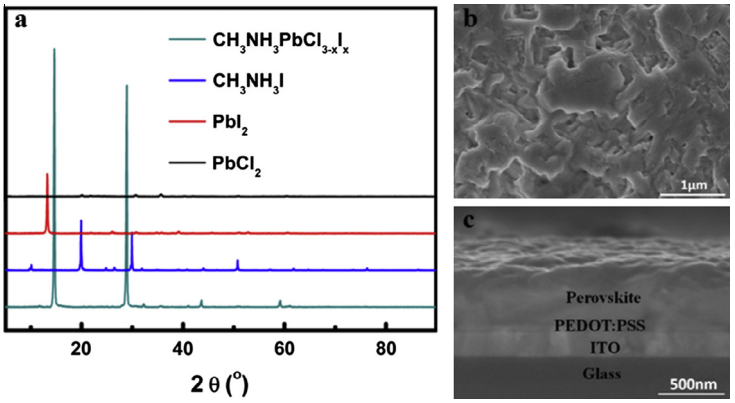

Fig. 5. (a) X-ray diffraction (XRD) spectra of $CH_3NH_3PbCl_{3-x}I_x$, CH_3NH_3I, PbI_2 and $PbCl_2$; (b) surface and (c) cross-section SEM images of the perovskite on the ITO substrate.

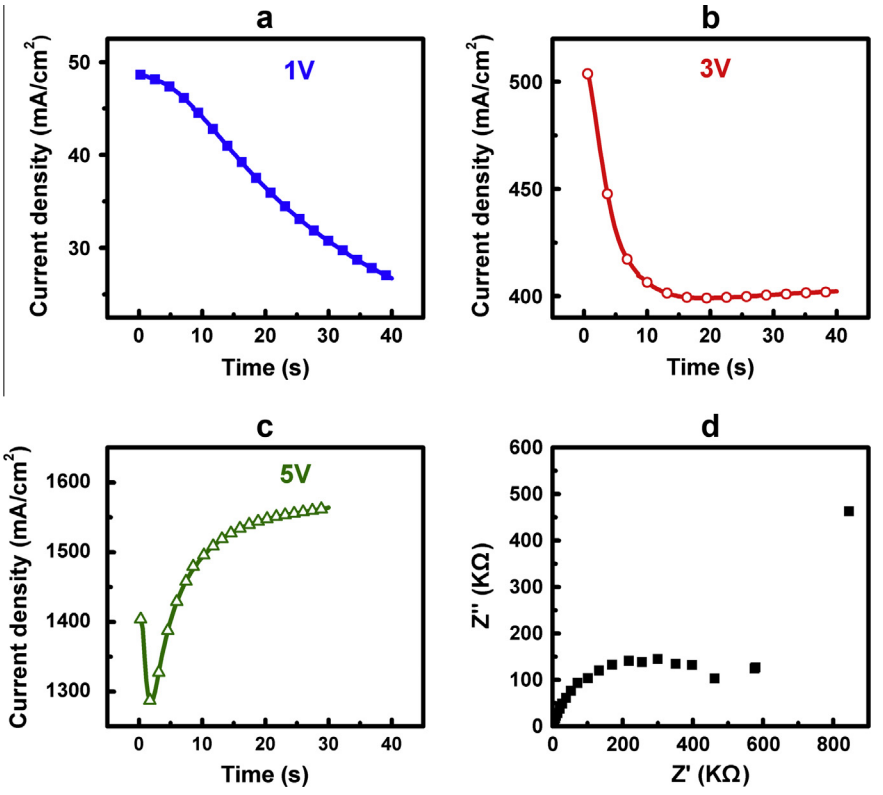

Fig. 6. Dark current transients under the applied bias of (a) 1 V, (b) 3 V and (c) 5 V. (d) The Nyquist plot of a fresh perovskite solar cell measured in the dark under 110 mV forward bias.

ions [33]. The ionic conductivity in perovskites was subsequently demonstrated in other materials as well, e.g. $CuPbI_3$ and $CuSnI_3$ [34,35]. Generally it is believed that interstitial ions are unlikely to be the major imperfections in the perovskite-type compounds. Therefore, the halide-ion migration in perovskites would proceed via a vacancy diffusion mechanism. The halide vacancies could be, for example, introduced by the addition of monovalent cations on the Pb site.

4. Conclusions

In summary, we found that the performance of perovskite solar cells could be strongly dependent on the external bias. By applying a 3 V bias on the device prior to the measurement and extending the scan range to −0.5 to 6 V, the PCE could be significantly increased from <1% to over 8%. Great attention should be paid to the effect of external bias on perovskite solar cells in future studies. Based on a range of experiments, including XRD, SEM, dark current transients, and impedance spectroscopy, we propose that ion motion under the external electric field might be responsible for our observation, although we cannot completely exclude other contributions from ferroelectricity or traps. Future work should aim at decreasing the ionic transport in perovskite solar cells, and hence improve the reproducibility and stability of the devices.

Acknowledgements

The Project (51273208) supported by National Natural Science Foundation of China and Hundred Talent Program of Chinese Academy of Sciences; the work was also supported by Zhejiang Provincial Natural Science Foundation of China (LR14E030002) and the Ningbo Natural Science Foundation of China (2012A610114). F.G. acknowledges the financial support of the European Commission under a Marie Curie Intra-European Fellowship for Career Development.

Appendix A. Supplementary material

Supplementary data associated with this article can be found, in the online version, at http://dx.doi.org/10.1016/j.orgel.2015.01.024.

References

[1] N.-G. Park, Organometal perovskite light absorbers toward a 20% efficiency low-cost solid-state mesoscopic solar cell, J. Phys. Chem. Lett. 4 (2013) 2423–2429.
[2] H.J. Snaith, Perovskites: the emergence of a new era for low-cost, high-efficiency solar cells, J. Phys. Chem. Lett. 4 (2013) 3623–3630.
[3] G. Hodes, Perovskite-based solar cells, Science 342 (2013) 317–318.
[4] A. Kojima, K. Teshima, Y. Shirai, T. Miyasaka, Organometal halide perovskites as visible-light sensitizers for photovoltaic cells, J. Am. Chem. Soc. 131 (2009) 6050–6051.

[5] M.M. Lee, J. Teuscher, T. Miyasaka, T.N. Murakami, H.J. Snaith, Efficient hybrid solar cells based on meso-superstructured organometal halide perovskites, Science 338 (2012) 643–647.

[6] J.H. Heo, S.H. Im, J.H. Noh, T.N. Mandal, C.-S. Lim, J.A. Chang, Y.H. Lee, H.-J. Kim, A. Sarkar, K. NazeeruddinMd, M. Gratzel, S.I. Seok, Efficient inorganic–organic hybrid heterojunction solar cells containing perovskite compound and polymeric hole conductors, Nat. Photonics 7 (2013) 486–491.

[7] J. Burschka, N. Pellet, S.-J. Moon, R. Humphry-Baker, P. Gao, M.K. Nazeeruddin, M. Gratzel, Sequential deposition as a route to high-performance perovskite-sensitized solar cells, Nature 499 (2013) 316–319.

[8] J.M. Ball, M.M. Lee, A. Hey, H.J. Snaith, Low-temperature processed meso-superstructured to thin-film perovskite solar cells, Energy Environ. Sci. 6 (2013) 1739–1743.

[9] M. Liu, M.B. Johnston, H.J. Snaith, Efficient planar heterojunction perovskite solar cells by vapour deposition, Nature 501 (2013) 395–398.

[10] G.E. Eperon, V.M. Burlakov, P. Docampo, A. Goriely, H.J. Snaith, Morphological control for high performance, solution-processed planar heterojunction perovskite solar cells, Adv. Funct. Mater. 24 (2014) 151–157.

[11] B. Conings, L. Baeten, C. De Dobbelaere, J. D'Haen, J. Manca, H.-G. Boyen, Perovskite-based hybrid solar cells exceeding 10% efficiency with high reproducibility using a thin film sandwich approach, Adv. Mater. 26 (2013) 2041–2046.

[12] Q. Chen, H. Zhou, Z. Hong, S. Luo, H.-S. Duan, H.-H. Wang, Y. Liu, G. Li, Y. Yang, Planar heterojunction perovskite solar cells via vapor-assisted solution process, J. Am. Chem. Soc. 136 (2014) 622–625.

[13] J.-Y. Jeng, Y.-F. Chiang, M.-H. Lee, S.-R. Peng, T.-F. Guo, P. Chen, T.-C. Wen, $CH_3NH_3PbI_3$ perovskite/fullerene planar-heterojunction hybrid solar cells, Adv. Mater. 25 (2013) 3727–3732.

[14] S. Sun, T. Salim, N. Mathews, M. Duchamp, C. Boothroyd, G. Xing, T.C. Sum, Y.M. Lam, The origin of high efficiency in low-temperature solution-processable bilayer organometal halide hybrid solar cells, Energy Environ. Sci. 7 (2014) 399–407.

[15] O. Malinkiewicz, A. Yella, Y.H. Lee, G.M. Espallargas, M. Graetzel, M.K. Nazeeruddin, H.J. Bolink, Perovskite solar cells employing organic charge-transport layers, Nat. Photonics 8 (2013) 128–132.

[16] J.T.-W. Wang, J.M. Ball, E.M. Barea, A. Abate, J.A. Alexander-Webber, J. Huang, M. Saliba, I. Mora-Sero, J. Bisquert, H.J. Snaith, R.J. Nicholas, Low-temperature processed electron collection layers of graphene/TiO_2 nanocomposites in thin film perovskite solar cells, Nano Lett. 14 (2013) 724–730.

[17] J. You, Z. Hong, Y. Yang, Q. Chen, M. Cai, T.-B. Song, C.-C. Chen, S. Lu, Y. Liu, H. Zhou, Y. Yang, Low-temperature solution-processed perovskite solar cells with high efficiency and flexibility, ACS Nano 8 (2014) 1674–1680.

[18] P. Docampo, J.M. Ball, M. Darwich, G.E. Eperon, H.J. Snaith, Efficient organometal trihalide perovskite planar-heterojunction solar cells on flexible polymer substrates, Nat. Commun. 4 (2013) 2761.

[19] C.C. Stoumpos, C.D. Malliakas, M.G. Kanatzidis, Semiconducting tin and lead iodide perovskites with organic cations: phase transitions, high mobilities, and near-infrared photoluminescent properties, Inorg. Chem. 52 (2013) 9019–9038.

[20] A. Dualeh, T. Moehl, N. Tétreault, J. Teuscher, P. Gao, M.K. Nazeeruddin, M. Grätzel, Impedance spectroscopic analysis of lead iodide perovskite-sensitized solid-state solar cells, ACS Nano 8 (2013) 362–373.

[21] J.M. Frost, K.T. Butler, F. Brivio, C.H. Hendon, M. van Schilfgaarde, A. Walsh, Atomistic origins of high-performance in hybrid halide perovskite solar cells, Nano Lett. 14 (2014) 2584–2590.

[22] J. Kim, G. Kim, Y. Choi, J. Lee, S. Heum Park, K. Lee, Light-soaking issue in polymer solar cells: photoinduced energy level alignment at the sol–gel processed metal oxide and indium tin oxide interface, J. Appl. Phys. 111 (2012) 114511.

[23] A. Mei, X. Li, L. Liu, Z. Ku, T. Liu, Y. Rong, M. Xu, M. Hu, J. Chen, Y. Yang, M. Grätzel, H. Han, A hole-conductor–free, fully printable mesoscopic perovskite solar cell with high stability, Science 345 (2014) 295–298.

[24] T. Baikie, Y. Fang, J.M. Kadro, M. Schreyer, F. Wei, S.G. Mhaisalkar, M. Graetzel, T.J. White, Synthesis and crystal chemistry of the hybrid perovskite $(CH_3NH_3)PbI_3$ for solid-state sensitised solar cell applications, J. Mater. Chem. A 1 (2013) 5628–5641.

[25] H.J. Snaith, A. Abate, J.M. Ball, G.E. Eperon, T. Leijtens, N.K. Noel, S.D. Stranks, J.T.-W. Wang, K. Wojciechowski, W. Zhang, Anomalous hysteresis in perovskite solar cells, J. Phys. Chem. Lett. 5 (2014) 1511–1515.

[26] T. McMahon, Dark current transients in thin-film CdTe solar cells, in: Photovoltaic Specialists Conference, IEEE, 2002, pp. 768–771.

[27] J. Fang, Y. Yang, L. Edman, Understanding the operation of light-emitting electrochemical cells, Appl. Phys. Lett. 93 (2008). 063503-063503-063503.

[28] P. Matyba, K. Maturova, M. Kemerink, N.D. Robinson, L. Edman, The dynamic organic p–n junction, Nat. Mater. 8 (2009) 672–676.

[29] S. van Reenen, P. Matyba, A. Dzwilewski, R.A.J. Janssen, L. Edman, M. Kemerink, A unifying model for the operation of light-emitting electrochemical cells, J. Am. Chem. Soc. 132 (2010) 13776–13781.

[30] Q. Pei, Yang, G. Yu, C. Zhang, A.J. Heeger, Polymer light-emitting electrochemical cells: in situ formation of a light-emitting p–n junction, J. Am. Chem. Soc. 118 (1996) 3922–3929.

[31] C. Ho, I. Raistrick, R. Huggins, Application of A–C techniques to the study of lithium diffusion in tungsten trioxide thin films, J. Electrochem. Soc. 127 (1980) 343–350.

[32] V. Gonzalez-Pedro, E.J. Juarez-Perez, W.-S. Arsyad, E.M. Barea, F. Fabregat-Santiago, I. Mora-Sero, J. Bisquert, General working principles of $CH_3NH_3PbX_3$ perovskite solar cells, Nano Lett. 14 (2014) 888–893.

[33] J. Mizusaki, K. Arai, K. Fueki, Ionic conduction of the perovskite-type halides, Solid State Ionics 11 (1983) 203–211.

[34] T. Kuku, Ionic transport and galvanic cell discharge characteristics of $CuPbI_3$ thin films, Thin Solid Films 325 (1998) 246–250.

[35] T.A. Kuku, A.M. Salau, Electrical conductivity of $CuSnI_3$, $CuPbI_3$ and $KPbI_3$, Solid State Ionics 25 (1987) 1–7.